Bulletin of Electrical Engineering and Informatics
Vol. 14, No. 6, December 2025, pp. 4232∼4243
ISSN: 2302-9285, DOI: 10.11591/eei.v14i6.9641

Thermal analysis of li-ion battery pack using phase change materials based on climate conditions

Ishak Mohammed Mokhtar Benounnane[1], Ahmed Wahid Belarbi[1], Mohammed El Bachir Ghribi[2]
[1]Applied Power Electronics Laboratory, Department of Electrical Engineering, Faculty of Electrical Engineering, University of Science and Technology of Oran–Mohamed Boudiaf, Oran, Algeria
[2]Independent researcher, Oran, Algeria

Article Info

Article history:

Received Dec 2, 2024
Revised Aug 9, 2025
Accepted Sep 27, 2025

Keywords:

Battery thermal management system
Finite element method
Lithium ion batteries
Phase change materials
Thermal conductivity
Thermal runaway

ABSTRACT

The development of lithium-ion batteries necessitates improved management of these systems, particularly with regard to thermal aspects. They operate optimally between 35 °C and 45 °C. Temperatures exceeding 50 °C accelerate cell aging, while those surpassing 60 °C can trigger thermal runaway, potentially leading to catastrophic failure. To mitigate these risks, phase change materials (PCMs) are employed in battery thermal management systems (BTMS). They absorb heat during charging or discharging, transitioning from solid to liquid, then release the stored energy during periods of low demand, solidifying to help regulate battery temperature. This study conducts a thermal analysis of a lithium-ion ($LiFePO_4$) battery pack delivering a 24 V load, using COMSOL MULTIPHYSICS software. The objective is to evaluate and compare the thermal behavior of different PCMs, RT27, Paraffin Wax 58-60, and HM030, against air as a baseline reference. Simulations are performed using the integrated finite element method (FEM), with a discharge rate of 4 C. A correlation is proposed between the choice of PCM and the climate in specific locations, with the choice being made based on the disparities in the results obtained.

Corresponding Author:

Ishak Mohammed Mokhtar Benounnane
Applied Power Electronics Laboratory, Department of Electrical Engineering, Faculty of Electrical Engineering
University of Science and Technology of Oran–Mohamed Boudiaf
Oran, Algeria
Email: ishakmohammed.mokhtarbenounnane@univ-usto.dz

1. INTRODUCTION

The development of renewable energy sources, particularly photovoltaic energy, as well as electric vehicles, has made batteries especially lithium-ion-based technologies a necessity [1]-[3]. Lithium-ion batteries are favored due to their high performance, significant storage capacity, and, most importantly, their longer lifespan compared to other battery types, in addition to their lower production costs. A lithium-ion battery stores three times more energy per unit volume than a lead-acid battery [4]-[6].

Severe impacts can lead to the explosion of lithium-ion batteries. To address this, various studies have been conducted on polymers designed to protect the battery pack [7]. In our case, we focus on thermal analysis and therefore directly use polyvinyl chloride (PVC) as the protective material. This type of battery typically consists of a sub-assembly of cells, with arrangements designed to achieve the desired voltage and current. An advanced battery management system (BMS) is crucial for efficient charging and monitoring of battery cells, especially for Li-ion batteries [8]-[10]. By accurately estimating the state of charge (SoC), the BMS

enhances energy efficiency while ensuring operational safety. Moreover, it plays a pivotal role in extending battery lifespan, optimizing performance, and mitigating critical risks such as overcharging, deep discharge, and thermal instability [11], [12]. However, these cells have several drawbacks, including significant thermal runaway during discharge, with a risk of explosion if the temperature exceeds 60 °C [13], [14]. This issue can be mitigated using a thermal management system (TMS) or by employing phase cange materials (PCMs) during the charging and discharging cycles of the battery [15]-[17]. The energy generated by the cells is directly absorbed by the PCM; consequently, the temperature of both the cells and the PCM gradually rises until it reaches the melting point of the PCM. At this stage, the PCM enters a phase where the absorbed energy is converted into latent heat, transitioning from a solid to a liquid state. Throughout this phase change, the system's temperature remains constant. Once the PCM has completely transitioned to the liquid state, if the cells continue to generate energy, the system temperature will begin to rise again [18].

To enhance thermal exchange capacity, a material with high thermal conductivity can be added to the PCM, resulting in a composite with increased thermal conductivity. An example is paraffin, which is typically combined with good thermal conductors such as graphite, semimetals, or metals [19], [20].

Recent advancements in battery thermal management systems (BTMS) have focused on improving the efficiency of PCMs through a range of innovative strategies. One of the most promising approaches is PCM microencapsulation, which involves enclosing PCM particles within protective shells. This technique enhances thermal conductivity, prevents leakage during phase transitions, and increases the heat exchange surface area, leading to more effective temperature regulation [21], [22]. Another significant method is the integration of nanofluids with PCMs. Nanofluids, composed of base fluids with suspended nanoparticles, can be combined with PCMs to boost both thermal conductivity and heat transfer rates. This hybrid configuration capitalizes on the high latent heat storage capacity of PCMs and the superior thermal conductivity of nanofluids, thereby enabling enhanced cooling performance [22], [23].

Additionally, various hybrid architectures combining PCMs with active thermal control systems such as cold plates, heat pipes, and fin-assisted air cooling have been extensively investigated in the literature [24]. These systems aim to synergize the passive thermal regulation offered by PCMs with the active heat dissipation mechanisms, resulting in improved thermal stability and enhanced overall performance of lithium-ion battery packs [25].

The use of lithium iron phosphate (LFP) batteries in combination with a passive cooling system based on PCM represents a solution that is both efficient and environmentally friendly. PCMs operate through a natural thermal cycle without requiring external energy input, making them completely carbon-neutral in terms of CO_2 emissions. However, while LFP batteries are more thermally stable and safer than other lithium-ion technologies, their overall environmental impact remains strongly dependent on the energy source used for charging. When powered by fossil-based electricity, indirect emissions can be significant, thereby affecting the system's overall carbon footprint. In this context, integrating a photovoltaic power supply emerges as a relevant strategy, helping to reduce emissions associated with electricity generation while ensuring effective thermal management. This combination supports compliance with international environmental standards and enhances the energy autonomy of the system [26].

This paper presents a comparison of different PCMs that can help regulate the temperature of a lithium-ion pack while limiting thermal runaway. In this case, the pack is composed of $A121$ lithium iron phosphate cell ($LiFePO_4$) cells, with eight cells arranged in series to achieve a voltage of 24 V and four in parallel to provide a current of 10 A, thus each branch delivers a nominal current of 2.5 A. The discharge rate of our battery is 4C, with a total current of 40 A. The paper provides a thermal analysis using COMSOL Multiphysics software to compare various PCM materials. The method employed for the calculations is the finite element method (FEM), integrated within COMSOL. The comparison is facilitated by maintaining a constant thermal discharge rate with the external environment across all scenarios. Advanced numerical techniques such as the FEM and the finite spectrum method (FSM) are widely used for the thermal analysis of cylindrical lithium-ion battery cells. FEM provides high spatial resolution by discretizing the cell geometry into finite elements, enabling precise modeling of anisotropic heat conduction across the various layers of the battery. In this study, COMSOL Multiphysics, which is based on FEM, was employed to develop a detailed thermal model of a cylindrical $LiFePO_4$ or LFP cell. The mesh was refined to $7370k$ elements, ensuring a sufficiently fine discretization to capture critical thermal gradients throughout the domain.

FSM, in contrast, is a hybrid numerical method that combines the computational efficiency of global spectral techniques with the geometric flexibility of the finite element framework. Locally, the solution, input

data, and geometry are represented using high-order Lagrange polynomials constructed on quadrature points. Globally, the domain is composed of an unstructured mesh of hexahedral elements, which may be deformed or geometrically non-conforming. This configuration allows FSM to achieve high accuracy while accommodating complex geometrical structures. Although FSM is well recognized for its analytical robustness and computational efficiency in solving certain heat transfer problems, it was not adopted in this work due to the already refined meshing strategy implemented with FEM. The chosen approach enables accurate evaluation of the thermal behavior, supporting the prediction of thermal runaway scenarios and the development of advanced thermal management systems. Spectral element method offers an efficient and highly accurate alternative for modeling static magnetic fields in complex devices such as electrical machines or magnetic shielding structures [27].

The simulation results illustrate the temperature distribution on the cell surface during a nominal discharge of 4C. Initially, air is used as a reference to compare with other materials. Next, the PCM in direct contact with the cells is replaced to observe the thermal behavior in each case and the effect of the material used. Among the materials tested is RT27, known for its good cooling efficiency, with performance linked to the average temperature along the external surface of the battery [28]. However, its low melting temperature represents a challenge: when the ambient temperature exceeds this point, the PCM's effectiveness is compromised. For this reason, it is essential to select a PCM whose melting temperature aligns with the expected ambient conditions, which vary according to geography, in order to ensure optimal cell operation while minimizing the risk of thermal runaway [29], [30]. The second material used is PARAFFIN WAX 58-60, a type of paraffin wax with a melting point between 58 °C and 60 °C, selected for its acceptable physical, mechanical, and thermal properties, as well as the fact that its melting temperature is close to the upper operating limit [31]. The third material is the $PCM\ HM030$, which has a melting temperature of around 30 °C, making it a complementary application to the other two materials [32].

The importance and originality of this research lie in the comprehensive comparative assessment of the thermal performance of multiple PCMs specifically adapted to a range of climatic conditions. While most previous studies have focused primarily on a single PCM or on standardized environmental settings, this study introduces an innovative approach by incorporating real-world climatic data to determine the most suitable PCM based on actual ambient temperature profiles. This methodology enables the selection of the most effective PCM according to realistic usage scenarios, thereby supporting the development of more reliable and context-specific thermal management strategies for lithium-ion battery systems.

2. METHOD

The selected lithium-ion cell is cylindrical, with a storage capacity of 2.5 Ah and a nominal voltage of 3.3 V when fully charged. Table 1 shows other specific technical data for the $A123$ battery used and Figure 1 illustrates its voltage profile as a function of the SoC. The cell has a diameter of 26 mm and a height of 65 mm. Figure 2 which also details the geometric dimensions of the pack used; only half of the pack is shown for symmetry reasons.

Table 1. Specific technical data for a single $A123$ cell

Parameter	Value
Cell dimensions	26×65 mm
Cell capacity (nominal/minimum) (0.5C rate)	2.5/2.4 Ah
Voltage (nominal)	3.3 V
Power	2600 W/kg
Maximum continuous discharge	50 A

In (1) demonstrates how to calculate the voltage of a cell as a function of its temperature, which has a strong dependence on this parameter. This variation is initially obtained through measurement and is then used in various simulations. The change in voltage drop or increase is also temperature-dependent. A reference temperature is generally selected to be 25 °C.

$$E(\text{SOC}, T) = E(\text{SOC}) + (T - T_{\text{ref}}) \frac{\partial E(\text{SOC})}{\partial T} \tag{1}$$

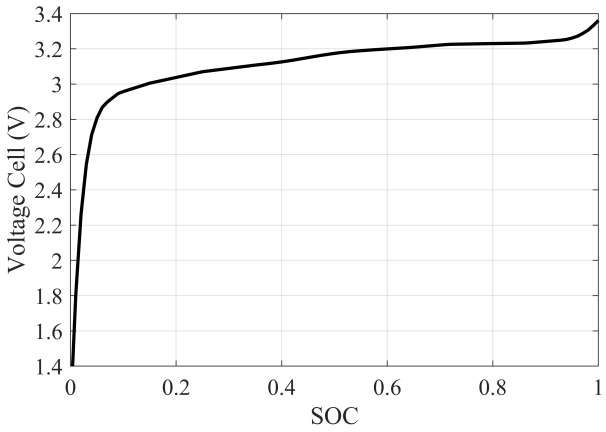

Figure 1. Caracterestic of voltage profile as function of the SoC

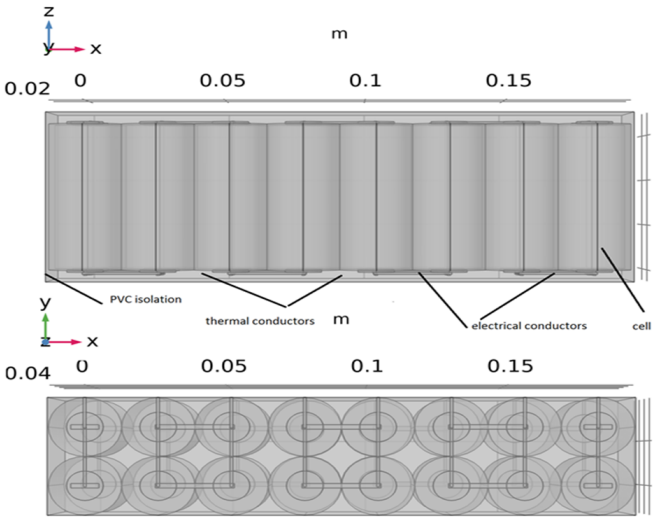

Figure 2. The geometric dimensions of the pack used

From (2) represents the voltage lose equation it combines the ideal OCV with the various overvoltage terms that represent the losses due to chemical and physical effects inside the cell, providing the actual voltage under operating conditions. The cell voltage depends not only on temperature and the SoC, but also on various voltage drops and overvoltage, whether due to ohmic or chemical effects. η_{act} represents the activation overvoltage, which is the voltage loss caused by the energy barrier that must be overcome for chemical reactions to occur. η_{conc} concentration overvoltage refers to the voltage loss due to mass transport limitations, such as the movement of ions and reactants within the cell. η_{IR} represents ohmic losses or ohmic drop, which is the voltage loss caused by the resistance to current flow within the cell conductive components.

$$E_{\text{cell}} = E_{\text{OCV}}(\text{SOC}, T) + \eta_{\text{act}} + \eta_{\text{conc}} + \eta_{\text{IR}} \tag{2}$$

In (3), models heat transfer within a solid, accounting for the temporal variation of temperature, conduction transfer, and internal or external heat sources. According to this equation, the heat exchange in the phase change material (PCM) in its solid state depends on its density, specific heat capacity, and, most critically, the heat absorbed by the cells and dissipated to the surrounding environment. In this state, heat is transferred by conduction without latent heat release or absorption. This equation allows the calculation of the

PCM temperature through the temperature derivative term. Here, the temperature increase is linear as long as no phase change occurs.

$$\rho c_p \frac{\partial T}{\partial t} + \rho c_p \, \mathbf{u} \cdot \nabla T + \nabla \cdot (-k \nabla T) = Q + Q_{\text{ted}} \tag{3}$$

In (4), which describes energy conservation for a fluid, is expressed as a function of temperature. This equation combines the two primary modes of heat transfer in a fluid: convection and conduction. The study of heat transport by the fluid considers the interaction between flow and heat exchange. The equation describes heat exchange when the material has changed phase to the liquid state. While the equation is similar to that used when the material is in the solid state, convection must now also be considered, as the PCM in its liquid state is mobile. In this case, heat transfer continues through conduction, but natural convection may become significant, especially if the PCM is in an open space, where fluid movement is induced by temperature differences. The term $\rho c_p \, \mathbf{u} \cdot \nabla T$ represents the convective term that models heat transported by fluid motion. It is proportional to the fluid density, specific heat capacity, and velocity field. The term $\nabla \cdot (-k \nabla T)$ represents conduction and describes how heat is transferred by conduction within the fluid. This term becomes significant when the fluid's thermal conductivity is high.

$$\rho c_p \, \mathbf{u} \cdot \nabla T + \nabla \cdot (-k \nabla T) = Q + Q_p + Q_{vd} \tag{4}$$

In (5) gives the effective specific heat capacity (Cp) of the PCM. The first term represents the contribution from the two phases, weighted by their fractions and specific heat capacities (Cp_1 and Cp_2). The second term adds the latent heat effect, where L is the latent heat of fusion. This equation captures both mechanisms solid and liquid state. The latent heat component becomes significant during the phase change, adding extra heat capacity without a temperature change.

$$c_p = \frac{1}{\rho} \left(\theta_1 \rho_1 c_{p,1} + \theta_2 \rho_2 c_{p,2} \right) + L_{(1 \to 2)} \, \frac{\partial \alpha_m}{\partial T} \tag{5}$$

From (6) calculates the effective density ρ of the PCM during the phase change, which is a weighted average of the densities of the two phases.

$$\rho = \theta_1 \rho_1 + \theta_2 \rho_2 \tag{6}$$

Table 2 presents the thermophysical properties of different materials such as air, RT27, and paraffin wax. These include thermal conductivity, specific heat capacity, and density, which are important for evaluating the ability of each material to store and transfer heat.

Table 2. PCM materials and their thermophysical properties

Material	Thermal conductivity (W/m·K)	Specific heat capacity (kJ/kg·K)	Density (kg/m^3)
Air	0.025	1.005	1.22
RT27	0.200	2.000	880
Paraffin Wax	0.206	2.100	920
HM030	0.200	1.932	880

3. RESULTS AND DISCUSSION

The thermal behavior of the lithium-ion battery pack was simulated using COMSOL Multiphysics, with air selected as the baseline thermal management medium. Figure 3 presents both the surface temperature distribution and the temporal evolution of temperatures across all cells during a 4C discharge. Air cooling is often used as a reference in thermal management studies due to its simplicity; however, its low thermal conductivity limits its ability to control temperature rise under high discharge rates. In Figure 3(a), the surface temperature of the cells increases from the initial ambient value of 25 °C to a range between 41 °C and 44 °C by the end of the discharge, indicating significant heat accumulation when air is used as the cooling medium. This distribution highlights the presence of localized hot spots, which can adversely affect the uniformity of cell performance and longevity. The temperature variation across the pack is attributed to cell positioning: peripheral cells, which are in direct contact with the external environment, remain cooler (around 41 °C),

whereas centrally located cells, more insulated from ambient air, reach higher temperatures (up to 44.3 °C). This gradient underscores the non-uniformity in heat dissipation across the battery pack.

Figure 3(b) presents the time-resolved temperature evolution during discharge. The plot distinguishes the average temperatures of the hottest and coolest cell groups, as well as their mean value, representing the overall pack temperature. While all cells start at 25 °C, disparities increase as the discharge progresses, with central cells retaining more heat due to limited exposure to ambient cooling. The inset in Figure 3(b) emphasizes a critical phase between 0.12 h and 0.22 h, during which thermal divergence between cell groups becomes more pronounced. This divergence clearly illustrates the challenge of relying solely on air cooling under high current loads, as it leads to uneven temperature distribution within the battery pack, potentially accelerating cell aging, reducing overall efficiency, and increasing the risk of thermal runaway in extreme cases.

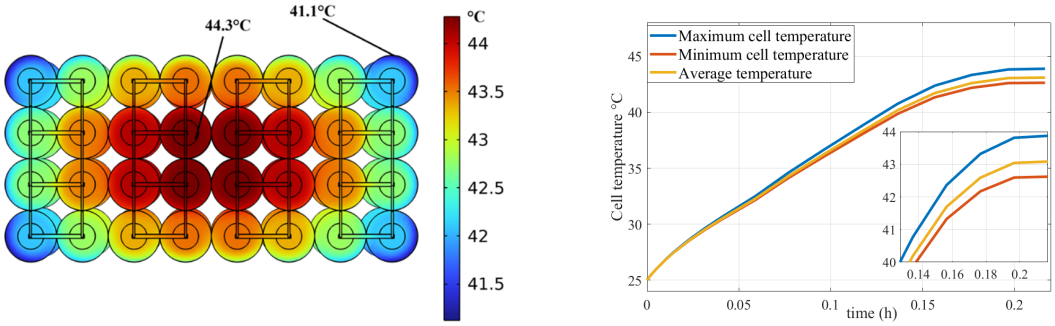

(a) (b)

Figure 3. Surface temperature distribution of lithium-ion cells after a 4C discharge with air; (a) temperature distribution for air and (b) real-time variation of maximum, minimum, and average temperatures across all cells with air

Figure 4, entitled surface temperature distribution of lithium-ion cells after a 4C discharge with PCM RT27; (a) temperature distribution for PCM RT27, (b) real-time variation of maximum, minimum, and average temperatures across all cells with PCM RT27, presents a detailed evaluation of the thermal behavior of the battery pack when cooled with the PCM RT27. In Figure 4(a), the results show a maximum cell temperature of 27.2 °C, with a remarkably uniform surface temperature distribution and negligible variation among cells. This homogeneity is primarily due to the latent heat absorption during the phase change from solid to liquid, which effectively limits temperature gradients and prevents localized hot spots. Considering that the initial temperature of the pack is 25 °C, if it were, for example, 30 °C, the phase change temperature of RT27 would already be exceeded, leading to reduced effectiveness. In such a situation, excess heat would no longer contribute to the phase transition but would directly increase the pack temperature, resulting in a less efficient thermal response and a potential rise beyond safe operational limits. RT27's narrow melting range makes it particularly effective in moderate climates or controlled environments where ambient temperatures remain below 27 °C. Compared to air cooling, which lacks thermal buffering capacity, RT27 provides superior temperature regulation and uniformity, as clearly illustrated in Figure 4(a), where minimal thermal deviation is observed between cells. Figure 4(b) complements this analysis by illustrating in real time the evolution of maximum, minimum, and average temperatures across all cells with PCM RT27. The maximum average cell temperature reaches 27.1 °C, while the minimum average is 27.04 °C, giving an overall pack average of 27.04 °C. This minimal temperature spread confirms the excellent thermal uniformity achieved with RT27. The inset in Figure 4(b) highlights a critical interval between 0.19 h and 0.20 h during which temperature stabilization is clearly observed, further demonstrating the PCM's capacity to maintain consistent and balanced thermal performance throughout the discharge process.

Paraffin wax 50–60 yielded better results compared to air, but less favorable outcomes than RT27: the maximum temperature of the battery pack reached 36.2 °C when the initial pack temperature was 25 °C. However, if the starting temperature is 35 °C, its performance surpasses that of RT27, as paraffin wax 58–60 can still absorb heat through a phase change. In terms of heat distribution across the cells, it is similar to that observed with air, but with a smaller temperature amplitude variation. In this case, as long as the melting

temperature of the PCM is not reached, its effect remains suboptimal.

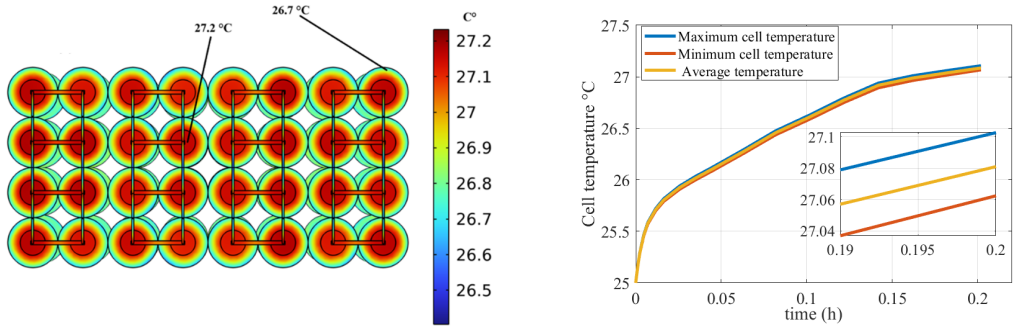

(a) (b)

Figure 4. Surface temperature distribution of lithium-ion cells after a 4C discharge with PCM RT27; (a) temperature distribution for PCM RT27 and (b) real-time variation of maximum, minimum, and average temperatures across all cells with PCM RT27

Figure 5 presents the thermal performance of the battery pack using paraffin wax 58–60 as PCM after a 4C discharge, a material widely reported in the literature for its higher melting point and delayed phase change behavior, which makes it more effective in high-temperature environments but less responsive in moderate conditions. Paraffin wax exhibits the highest melting point, typically ranging from 58 °C to 60 °C, which delays its phase transition until more significant thermal loads are encountered. This property makes it particularly suitable for battery systems operating in warmer environments or under high discharge rates. While its thermal conductivity and latent heat capacity are comparable to those of RT27, paraffin 50–60 offers a substantial advantage in terms of cost-effectiveness and widespread availability, making it an attractive option for large-scale thermal management applications.

In Figure 5(a), the surface temperature distribution shows a maximum of 36.1 °C and a minimum of 35.1 °C, reflecting a moderate thermal gradient. This behavior is linked to the fact that paraffin wax 58–60 starts absorbing heat significantly only when approaching its melting range. Figure 5(b) supports this observation, with a pack average of 35.4 °C and a slight temperature divergence between cell groups during the interval 0.19–0.20 h, highlighting the importance of aligning PCM melting characteristics with the system's thermal load and operating conditions. In contrast, RT27, a commercial PCM engineered with a narrow melting range around 27 °C, delivers superior thermal stability and encapsulation performance, which is particularly beneficial for compact BTMS architectures requiring precise temperature control. Therefore, the choice between paraffin 50–60 and RT27 should consider not only thermal performance but also economic constraints, scalability, and compatibility with existing battery systems. These findings highlight the need for an integrated selection approach when designing PCMs for energy storage systems exposed to varying climatic conditions.

Figure 6 presents the thermal performance of the battery pack when cooled with PCM HM030 after a 4C discharge. According to the results, the maximum temperature of the battery pack reached 29.6 °C, corresponding to the phase change threshold of the material. At this point, the temperature remains stable as the latent heat of fusion absorbs the excess thermal energy generated during the discharge. If the PCM is not entirely melted, the pack temperature does not increase further, indicating effective thermal buffering. Beyond simply limiting the peak temperature, HM030 ensures uniform heat distribution across all cells, thereby minimizing temperature gradients that could lead to localized overheating or performance inconsistencies. This homogeneous thermal behavior plays a critical role in maintaining operational safety, enhancing system reliability, and extending the overall lifespan of the battery pack. Figure 6(a) confirms this effect, illustrating a smooth and consistent surface temperature distribution across the entire cell module following the discharge cycle. Figure 6(b) illustrates, in real time, the maximum, minimum, and average temperatures recorded across all cells with PCM HM030. In this case, the maximum average cell temperature reaches 29.5 °C, while the minimum average is 29.4 °C, resulting in a pack average of 29.54 °C. This extremely low thermal gradient reflects the effective phase change behavior of HM030, which operates optimally within this temperature range, ensuring uniform heat absorption across the pack. The inset in Figure 6(b) highlights a critical phase between

0.19 h and 0.20 h, during which the temperature difference between cells remains minimal, demonstrating the high level of thermal uniformity provided by HM030 under high discharge conditions.

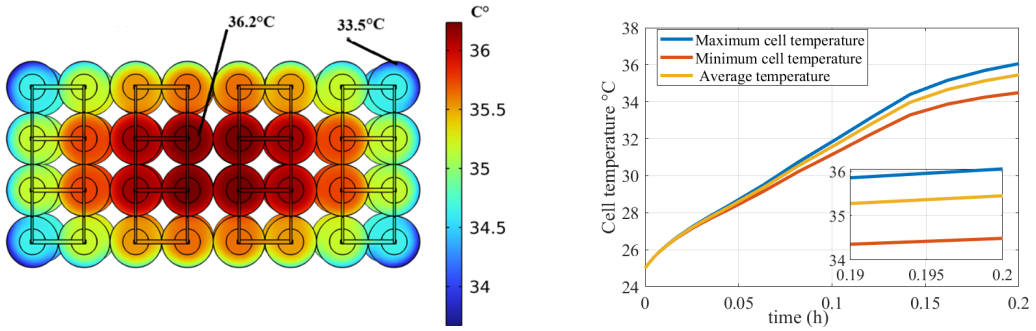

(a) (b)

Figure 5. Surface temperature distribution of lithium-ion cells after a 4C discharge with PCM Paraffin Wax 58–60; (a) temperature distribution for PCM Paraffin Wax 58–60 and (b) real-time variation of maximum, minimum, and average temperatures across all cells with PCM Paraffin Wax 58–60

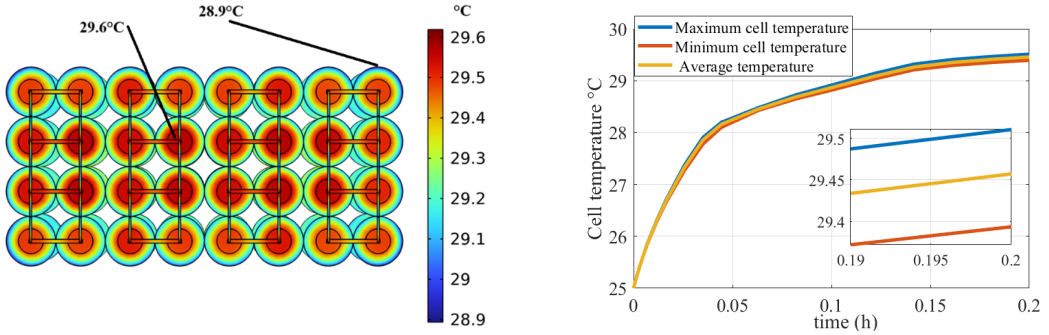

(a) (b)

Figure 6. Surface temperature distribution of lithium-ion cells after a 4C discharge with PCM HM030; (a) temperature distribution for PCM HM030 and (b) real-time variation of maximum, minimum, and average temperatures across all cells with PCM HM030

This study compares several PCMs with different melting temperatures, with the aim of prioritizing one over the others according to the external climate. For cold climates, a PCM with a low melting temperature is selected, as high-load operation can quickly raise cell temperatures; thus, a lower melting point ensures optimal performance. For hot climates, a PCM with a melting point close to the cell's stability limit is chosen to maintain effectiveness under significantly high ambient temperatures. For temperate climates, a PCM offering a balanced compromise between these two extremes is selected. According to Figure 7, which presents the variation of pack voltage over time, the voltage is proportional to the pack temperature. Air exhibits a higher voltage compared to the PCMs evaluated, as the cell temperature is highest in this case. In this discharge scenario, when air is used as the medium, the total power transmitted is equal to the product of voltage and current, resulting in W. In contrast, with RT27 as the PCM, the transmitted power is 251.42 W.

Figure 8 shows the maximum temperature measured over the course of a year for various North American cities (Boston, Dallas, New York, and New Orleans), with the different PCM used. The purpose of this graph is to identify the most suitable PCM for each case, with the objective that the external temperature never exceeds the melting point of the PCM. This approach allows for the selection of a PCM that is always adapted to the local climate conditions. In Boston, the maximum temperature measured never exceeds 29 °C in the shade, making HM030 an appropriate choice. In this case, the PCM will not melt, as the external temperature

remains below its melting point, while the battery generates enough heat to facilitate its melting. However, for Dallas, the maximum temperature measured throughout the year exceeds the melting point of both HM030 and RT27, leading to the melting of the PCM. In this scenario, the most suitable PCM is PARAFFINEWAX 50-60 as its melting point is above 55 °C.

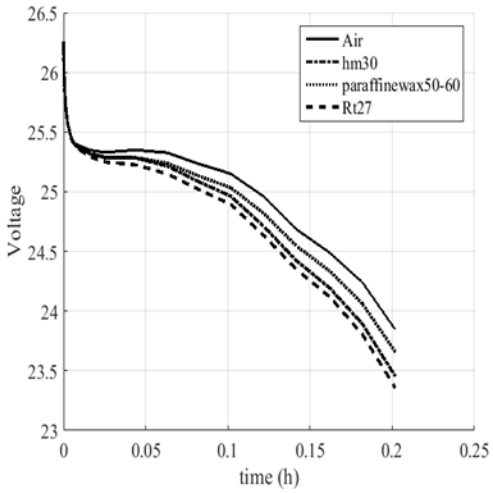

Figure 7. Variation of the pack's average voltage over time for different PCM materials used

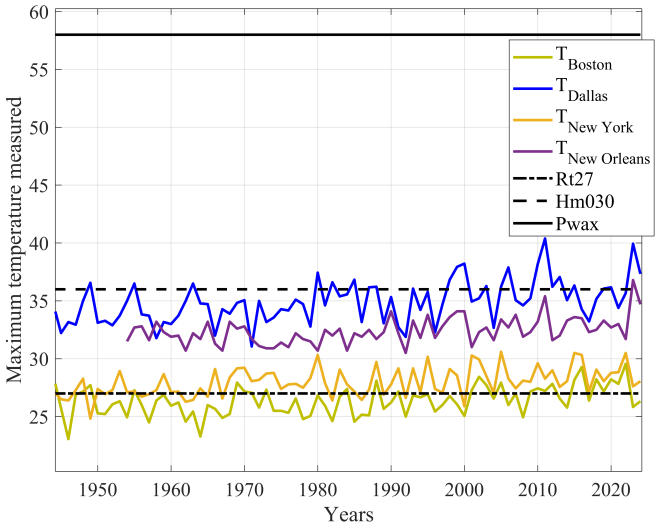

Figure 8. The maximum temperature measured over the course of a year for various North American cities with the different PCM [33]

The environmental impact and scalability of PCMs such as HM03.0, paraffin wax 50–60, and RT27 are critical considerations for BTMS. Paraffin-based PCMs like RT27 and 50–60 are economically viable and recyclable; however, their petroleum-based origin raises significant sustainability concerns [34], [35]. HM03.0 demonstrates superior thermal performance, but its formulation with specific chemical additives may reduce its recyclability [36]. While paraffin PCMs benefit from well-established manufacturing chains that support large-scale deployment [1], HM03.0 may face limitations in cost-efficiency and raw material availability [37]. Advancing hybrid PCMs that combine favorable thermal characteristics with eco-friendly profiles could improve both the environmental sustainability and scalability of BTMS technologies.

4. CONCLUSION

This paper presents a comparative study of different thermal conductors used to dissipate heat generated by various systems. In this case, the system in question is a cell pack consisting of 32 lithium-ion cells, providing a nominal voltage of 3.3 V per cell at full charge. The pack operates at 24 V, with 8 cells connected in series and 4 in parallel. The study considers cell discharge at a current of 4C. The materials used are PCMs, which stabilize temperature through phase transitions at their melting points. These materials are generally composed, at least partially, of paraffin, a substance widely used in this field. As a baseline, air is used in place of thermally conductive materials. The results show that, under the discharge current applied, the heat generated by the cells is insufficient to completely melt the PCMs. Consequently, temperature stabilization occurs only when the melting process begins. If the melting point is not reached, it indicates that the battery has completed its discharge, as is observed with paraffin wax 58–60. The choice of PCM depends on the ambient climate: RT27 is ideal when external temperatures rarely exceed 27 °C, whereas paraffin wax 58–60 is better suited for hotter environments. HM30 offers a compromise between the two. Therefore, as long as ambient temperature does not cause premature PCM melting, the material can effectively help limit battery temperature and ensure protection.

The approach proposed in this study takes into account not only the physical properties of the selected PCM but also the specific external climatic conditions the material is expected to face. The primary objective is to ensure that PCM melting is triggered solely by internal heat generation within the battery pack during operation, and not by ambient temperature.

To this end, a high discharge current of 4C is employed, representing a typical upper operational limit, in order to evaluate the thermal endurance of the battery system. However, future work could investigate more realistic load profiles, such as those encountered in photovoltaic energy storage systems, where charge–discharge cycles involve lower but fluctuating current levels.

Moreover, integrating advanced numerical models with experimental validation would greatly improve the precision of PCM selection for specific battery configurations and real-world applications. While this study offers valuable insights into the climate-dependent thermal performance of PCMs, it remains limited by the scope and duration of the simulations, which do not fully capture all transient thermal phenomena.

FUNDING INFORMATION

Authors state no funding involved

AUTHOR CONTRIBUTIONS STATEMENT

This journal uses the Contributor Roles Taxonomy (CRediT) to recognize individual author contributions, reduce authorship disputes, and facilitate collaboration.

Name of Author	C	M	So	Va	Fo	I	R	D	O	E	Vi	Su	P	Fu
Ishak Mohammed Mokhtar Benounnane	✓	✓	✓	✓		✓		✓	✓					
Ahmed Wahid Belarbi					✓		✓		✓	✓		✓	✓	✓
Mohammed El Bachir Ghribi	✓		✓	✓				✓	✓		✓			

C : **C**onceptualization
M : **M**ethodology
So : **So**ftware
Va : **Va**lidation
Fo : **Fo**rmal Analysis
I : **I**nvestigation
R : **R**esources
D : **D**ata Curation
O : Writing - **O**riginal Draft
E : Writing - Review & **E**diting
Vi : **Vi**sualization
Su : **Su**pervision
P : **P**roject Administration
Fu : **Fu**nding Acquisition

CONFLICT OF INTEREST STATEMENT

Authors state no conflict of interest.

DATA AVAILABILITY

Derived data supporting the findings of this study are available from the corresponding author [IMMB] on request.

REFERENCES

[1] S. Sudaryanto *et al.*, "Enhancing the electrochemical performance of next-generation 5 V class Li-ion batteries using LiPF6/LiBOB mixed salt electrolyte," *Journal of Applied Research and Technology*, vol. 22, no. 5, pp. 662–673, 2024, doi: 10.22201/icat.24486736e.2024.22.5.2374.

[2] B. Diouf and R. Pode, "Potential of lithium-ion batteries in renewable energy," *Renewable Energy*, vol. 76, pp. 375–380, 2015, doi: 10.1016/j.renene.2014.11.058.

[3] T. Horiba, "Lithium-ion battery systems," *Proceedings of the IEEE*, vol. 102, no. 6, pp. 939–950, 2014, doi: 10.1109/JPROC.2014.2319832.

[4] H. Budde-Meiwes *et al.*, "A review of current automotive battery technology and future prospects," Proceedings of the Institution of Mechanical Engineers, *Part D: Journal of Automobile Engineering*, vol. 227, no. 5, pp. 761–776, 2013, doi: 10.1177/0954407013485567.

[5] A. Khaligh and Z. Li, "Battery, ultracapacitor, fuel cell, and hybrid energy storage systems for electric, hybrid electric, fuel cell, and plug-in hybrid electric vehicles: State of the art," *IEEE Transactions on Vehicular Technology*, vol. 59, no. 6, pp. 2806–2814, 2010, doi: 10.1109/TVT.2010.2047877.

[6] Y. Ding, Z. P. Cano, A. Yu, J. Lu, and Z. Chen, "Automotive Li-ion batteries: Current status and future perspectives," *Electrochemical Energy Reviews*, vol. 2, no. 1, pp. 1–28, 2019, doi: 10.1007/s41918-018-0022-z.

[7] S. Kaleg *et al.*, "Unsaturated polyester resin/aluminum tri-hydroxide added with short glass fiber for battery box," *Journal of Applied Research and Technology*, vol. 21, no. 3, pp. 457–470, 2023, doi: 10.22201/icat.24486736e.2023.21.3.1904.

[8] S. S. Kadlag, M. P. Thakre, R. Mapari, R. Shriwastava, P. C. Tapre, and D. P. Kadam, "A novel pulse charger with intelligent battery management system for fast charging of electric vehicle," *Bulletin of Electrical Engineering and Informatics*, vol. 12, no. 3, pp. 1388–1396, 2023, doi: 10.11591/eei.v12i3.4890.

[9] A. Tomaszewska *et al.*, "Lithium-ion battery fast charging: A review," *eTransportation*, vol. 1, Aug. 2019, doi: 10.1016/j.etran.2019.100011.

[10] G.-L. Zhu *et al.*, "Fast Charging Lithium Batteries: Recent Progress and Future Prospects," *Small*, vol. 15, no. 15, p. 1805389, Mar. 2019, doi: 10.1002/smll.201805389.

[11] M. Lagraoui, A. Nejmi, H. Rayhane, and A. Taouni, "Estimation of lithium-ion battery state-of-charge using an extended Kalman filter,"*Bulletin of Electrical Engineering and Informatics*, vol. 10, no. 4, pp. 1759–1768, 2021, doi: 10.11591/eei.v10i4.3082.

[12] R. Restaino and W. Zamboni, "Comparing particle filter and extended Kalman filter for battery state-of-charge estimation," *IECON 2012 - 38th Annual Conference on IEEE Industrial Electronics Society*, 2012, pp. 4018–4023, doi: 10.1109/IECON.2012.6389247.

[13] R. Lioger *et al.*, "Study of the boiling of a dielectric fluid in a vertical mini-channel: application to the thermal control of battery packs (in France: Étude de l'ébullition d'un fluide diélectrique en mini-canal vertical: application au contrôle thermique des packs batteries)," Thèse de doctorat, Université Grenoble Alpes, 2023, disponible à, [Online]. Available: https://theses.hal.science/tel-04127164.

[14] B. Xu, J. Lee, D. Kwon, L. Kong, and M. Pecht, "Mitigation strategies for Li-ion battery thermal runaway: A review," *Renewable and Sustainable Energy Reviews*, vol. 150, p. 111437, 2021, doi: 10.1016/j.rser.2021.111437.

[15] X. Zhang, Z. Li, L. Luo, Y. Fan, and Z. Du, "A review on thermal management of lithium-ion batteries for electric vehicles," *Energy*, vol. 238, p. 121652, 2022, doi: 10.1016/j.energy.2021.121652.

[16] M. M. Farid, A. M. Khudhair, S. A. K. Razack, and S. Al-Hallaj, "A review on phase change energy storage: Materials and applications," *Energy Conversion and Management*, vol. 45, no. 9–10, pp. 1597–1615, 2004, doi: 10.1016/j.enconman.2003.09.015.

[17] C. Nainika, P. Balamurugan, J. L. F. Daya, and V. A. krishnan, "Real driving cycle-based SoC and battery temperature prediction for electric vehicles using AI models," *Journal of Applied Research and Technology*, vol. 22, no. 3, pp. 351–361, 2024, doi: 10.22201/icat.24486736e.2024.22.3.2453.

[18] K. Pielichowska and K. Pielichowski, "Phase change materials for thermal energy storage," *Progress in Materials Science*, vol. 65, pp. 67–123, 2014, doi: 10.1016/j.pmatsci.2014.03.005.

[19] R. Gulfam, P. Zhang, and Z. Meng, "Advanced thermal systems driven by paraffin-based phase change materials – A review," *Applied Energy*, vol. 238, pp. 582–611, 2019, doi: 10.1016/j.apenergy.2019.01.114.

[20] B. Buonomo, D. Ercole, O. Manca, and F. Menale, "Thermal cooling behaviors of lithium-ion batteries by metal foam with phase change materials," *Energy Procedia*, vol. 148, pp. 1175–1182, 2018, doi: 10.1016/j.egypro.2018.08.024.

[21] G. V. N. Trivedi, R. Barbade, and R. Parameshwaran, "A review on preparation, characterisation and applications of microencapsulated phase change material slurries for thermal fluid and energy systems," *International Journal of Hydromechatronics*, vol. 8, no. 2, pp. 148–182, 2025, doi: 10.1504/IJHM.2025.145773.

[22] M. G. Kibria *et al.*, "A review on composite phase change materials and fins-based Li-ion battery thermal management systems with design perspectives and future outlooks," *Energy & Fuels*, vol. 38, no. 15, pp. 13637–13660, 2024, doi: 10.1021/acs.energyfuels.4c02062.

[23] M. Asim and F. R. Siddiqui, "Hybrid nanofluids—next-generation fluids for spray-cooling-based thermal management of high-heat-flux devices," *Nanomaterials*, vol. 12, no. 3, p. 507, 2022, doi: 10.3390/nano12030507.

[24] Z. Lyu, J. Su, Z. Li, X. Li, H. Yan, and L. Chen, "A compact hybrid battery thermal management system for enhanced cooling," *arXiv*, 2024, doi: 10.48550/arXiv.2412.00999.

[25] A. Tang *et al.*, "Characterization and experimental assessment of hybrid cooling strategy for lithium-ion batteries by integrating microencapsulated phase change materials," *International Journal of Heat and Mass Transfer*, vol. 224, p. 125389, 2024, doi: 10.1016/j.ijheatmasstransfer.2024.125389.

[26] A. Ansari and M. H. Shojaeefard, "A comprehensive review of phase change materials and their applications in battery thermal

management systems," *Automotive Science and Engineering*, vol. 14, no. 1, pp. 1–20, 2024, doi: 10.22068/ase.2024.695.
[27] P. F. Fischer and H. M. Tufo, "High-performance spectral element algorithms and implementations," *Argonne National Laboratory (ANL)*, IL, USA, 1999.
[28] A. Arumugam, B. Buonomo, P. Romano, and O. Manca, "Numerical investigation on liquid cooling of batteries in phase change materials," *9th European Thermal Sciences Conference (Eurotherm 2024)*, vol. 2766, no. 1, p. 012050, 2024, doi: 10.1088/1742-6596/2766/1/012050.
[29] S. K. Maknikar and A. M. Pawar, "Application of phase change material (PCM) in battery thermal management system (BTMS): A critical review," *Materials Today: Proceedings*, 2023, doi: 10.1016/j.matpr.2023.08.329.
[30] A. Babapoor, M. Azizi, and G. Karimi, "Thermal management of a Li-ion battery using carbon fiber-PCM composites," *Applied Thermal Engineering*, vol. 82, pp. 281–290, 2015, doi: 10.1016/j.applthermaleng.2015.02.068.
[31] B. Kudachi, S. Pathan, and N. Varkute, "Experimental study of solar water heater system using phase change material," *International Conference on Technologies for Energy, Agriculture, and Healthcare*, Apr. 2024.
[32] G. Chen, Y. Shi, and Y. Yu, "A thermal management design using phase change material in embedded finned shells for lithium-ion batteries," *International Journal of Heat and Mass Transfer*, vol. 229, p. 125680, 2024, doi: 10.1016/j.ijheatmasstransfer.2024.125680.
[33] NOAA National Centers for Environmental Information, "Climate at a Glance: City Time Series," Published in Nov. 2024, available at: https://www.ncei.noaa.gov/access/monitoring/climate-at-a-glance/city/time-series. (Accessed: Dec. 1, 2024).
[34] H. Jin, J. Cui, C. Zhu, Y. Li, Y. Chen, and Y. Su, "Preparation and performance study of paraffin composite phase change thermal storage material," *Conference Series, Volume 3080, The 11th International Conference on Applied Materials and Manufacturing Technology (ICAMMT 2025)*, vol. 3080, p. 012143, 2025, doi: 10.1088/1742-6596/3080/1/012143.
[35] A. Sharma, V. V. Tyagi, C. R. Chen, and D. Buddhi, "Review on thermal energy storage with phase change materials and applications," *Renewable and Sustainable Energy Reviews*, vol. 13, no. 2, pp. 318–345, 2009, doi: 10.1016/j.rser.2007.10.005.
[36] L. F. Cabeza, A. Castell, M. Medrano, I. Martorell G. Pérez, and I. Fernández, "Experimental study on the performance of insulation materials in Mediterranean construction," *Energy and Buildings*, vol. 42, no. 5, pp. 630-636, 2010, doi: 10.1016/j.enbuild.2009.10.033.
[37] S. Al-Hallaj and J. R. Selman, "Thermal modeling of secondary lithium batteries for electric vehicle/hybrid electric vehicle applications," *Journal of Power Sources*, vol. 110, no. 2, pp. 341–348, 2002, doi: 10.1016/S0378-7753(02)00196-9.

BIOGRAPHIES OF AUTHORS

Ishak Mohammed Mokhtar Benounnane was born in Oran Algeria in 1998. He is currently a Ph.D. student at the University of Science and Technology of Oran, Algeria, He holds a Master's degree in Industrial Electrical Engineering. Member of the Laboratory of Applied Power Electronics (LEPA). His main research interests are battery thermal management system and renewable energies. He can be contacted at email: ishakmohammed.mokhtarbenounnane@univ-usto.dz.

Ahmed Wahid Belarbi was born in 1965. He received the B.E. degree in electrical engineering from University of Science and Technology of Oran in 1989, the Ph.D. degree from Paul Sabatier University, Toulouse III, French, in 1994. He works at University of Science and Technology of Oran, Algeria since 1996; he is a professor of the Faculty of Electrical Engineering and director of Applied Power Electronic Laboratory. His research interests are high voltage, electric network, insulating materials, and renewable energy. He can be contacted at email: ahmedwahid.belarbi@univ-usto.dz.

Mohammed El Bachir Ghribi was born in 1999 in Oran (Algeria), obtained his Ph.D. in 2025 in electrical control at the University of Science and Technology of Oran (USTO). His research mainly focuses on power systems, power electronics, and renewable energy. He can be contacted at email: mohammedelbachir.ghribi@gmail.com.